WILEY-VCH

DOI: 10.1002/ ((please add manuscript number))
Article type: Full Paper

Electric Field Induced Molecular Assemblies Showing Different Nanostructures and Distinct Emission Colors

Yun Ma,[a,b] Weiwei Zhao,[b] Pengfei She,[b] Suyi Liu,[b] Liang Shen,[b] Xiangling Li,[b] Shujuan Liu,[b] Qiang Zhao,[b] Wei Huang,[b] and Wai-Yeung Wong*[a,c]*

[a] Dr. Y. Ma, Prof. Dr. W.-Y. Wong
Department of Applied Biology and Chemical Technology, The Hong Kong Polytechnic University, Hung Hom, Hong Kong, P. R. China. E-mail: wai-yeung.wong@polyu.edu.hk
[b] Dr. Y. Ma, Dr. W. W. Zhao, Mr. P. F. She, Mr. S. Y. Liu, Mr. L. Shen, Mr. X. L. Li, Prof. Dr. S. J. Liu, Prof. Dr. Q. Zhao, Prof. Dr. W. Huang
Key Laboratory for Organic Electronics & Information Displays (KLOEID) and Institute of Advanced Materials (IAM), Nanjing University of Posts & Telecommunications (NUPT), 9 Wenyuan Road, Nanjing 210023, Jiangsu, P. R. China. E-mail: iamqzhap@njupt.edu.cn
[c] Prof. Dr. W.-Y. Wong
The Hong Kong Polytechnic University Shenzhen Research Institute, Shenzhen, P. R. China.

Keywords: supramolecular chemistry, molecular assembly, metal-metal interactions, electric field, photoluminescence

Application of external stimuli in self-assembly processes would offer greater degrees of freedom to regulate the supramolecular nanostructures and functions of self-assembling molecules. In particular, the utilization of electric field to control molecular self-assembly is of fundamental significance, and it contributes to the development of applications in nanofabrication and optoelectronic fields. Here we study the self-assembly of an anionic platinum complex ($[Pt(tfmpy)(CN)_2]^-Bu_4N^+$, tfmpy = 2-(4-(trifluoromethyl)phenyl)pyridine)) in the absence or presence of an electric field. Scanning electron microscopy (SEM) and transmission electron microscopy (TEM) images demonstrated an interesting morphological transformation from rod-like to flower-shaped nanoaggregate structures. For rod-like nanostructure, selected area electron diffraction (SAED) and powder X-ray diffraction (PXRD) analysis suggested that that the Bu_4N^+ cations are squeezed between adjacent platinum(II) complex anions, forming alternating layers of two ions. In addition, SAED result suggested the flower-shaped nanoaggregate is constructed by a layer-by-layer packing

through the formation of Pt···Pt and π-π stacking interactions. Importantly, confocal fluorescence imaging showed that these two different stable assemblies possess distinct emission colors and lifetimes. This unique feature might be useful in various optoelectronic applications including data recording, anti-counterfeiting, smart windows, etc.

1. Introduction

Supramolecular nanostructures created by molecular assemblies have attracted considerable interest due to their rich aggregation structures and unique optical properties.[1] The introduction of external stimuli to manipulate supramolecular architectures would provide more possibilities for preparing self-assembled functional nanostructures with different morphologies and optoelectronic properties. In this respect, light,[2] magnetic field[3] and electric field[4] have drawn much attention because they can be delivered remotely and instantaneously to the assembled systems. Among them, electric field can be considered as a useful tool for obtaining different supramolecular nanostructures. For example, Stupp and coworkers prepared two compounds with opposite charges to form an ordered membrane under an electric field.[4b] Sun and coworkers demonstrated an *in situ* electrically driven cation exchange process for the construction of an individual sulfide supramolecular architecture.[4c] Although self-assembly by applying an electric field has been achieved, the investigations on the changes of their optical properties induced by morphological variations are rare. To date, only few examples of two stable assemblies with distinct morphological and optical properties have been reported.[5] Particularly, examples of two different supramolecular nanostructures exhibiting distinct emission colors are very rare. The drastic emission color changes between two nanoaggregate structures would be useful in recognizing the morphological transformation of molecular materials and in realizing different optoelectronic applications. Moreover, the study on the effect of changing the voltage or the electrode on the formation of different nanostructures is important to obtain deep insights into the assembling processes.

Platinum(II) complexes have attracted broad research interest due to their intriguing optical and facile self-assembly properties, associated with metal-metal and π-π stacking interactions.[6] Different supramolecular architectures have been obtained by modifying the chemical structures of platinum(II) complexes and changing the solvent composition.[5,6] Although distinct morphologies have been realized by a class of amphiphilic anionic platinum(II) complexes, those nanostructures exhibit the same emission color due to the metal to metal interactions.[5a] Recently, a class of anionic platinum(II) complexes has been shown to exhibit monomer emission in the solid state.[7] It is because the Pt···Pt interactions, which normally result in aggregate formation, are suppressed due to the existence of bulky counterion. This feature makes this class of anionic platinum(II) complexes potential candidates to realize different nanostructures with distinct emission colors in the absence or presence of an external stimulus.

At first glance, we have tried to achieve this goal by changing the solvent compositions in the self-assembly processes of an anionic platinum(II) complex $[Pt(tfmpy)(CN)_2]^-Bu_4N^+$ (**1**) (tfmpy = 2-(4-(trifluoromethyl)phenyl)pyridine). As shown in Figure S1, different nanostructures can be obtained by this method, but all these supramolecular structures exhibit the same green emission color. Consequently, it seems that the spontaneous self-assembly into a state of thermodynamic equilibrium cannot achieve the goal of different nanostructures with distinct emission colors. Therefore, it is envisioned that the out-of-equilibrium self-assembled nanostructure may exhibit different morphology and photoluminescence (PL) property under an external stimulus. In such case, applying an external stimulus to change the spatial position of complex and counterion might lead to significant variations in their supramolecular architectures and optical properties. Considering the ionic characteristic of anionic platinum(II) complexes, electric field would be a perfect choice to induce the molecular assemblies. Herein, complex **1** has been prepared as the building block for supramolecular assemblies (**Figure 1**a). By slow evaporation of a CH_3CN solution of **1**, the

mononuclear anionic platinum(II) complex was found to exhibit a strong tendency toward the formation of a nanorod structure with an intense green emission. On the other hand, by applying an electric field in a CH_3CN solution of **1**, a flower-like nanoaggregate structure was formed, which was rarely seen in small organic molecules and metal complexes.[8] Moreover, it was found that this flower-like nanostructure displayed a strong orange photoluminescence. Therefore, two stable nanostructural assemblies with distinct emission colors have been realized. In addition, the influence of electric field on the assembly process has been investigated. The results revealed that the surface roughness of various electrodes plays significant roles in the formation of different supramolecular structures.

2. Results and Discussion

2.1. Synthesis and Characterization

The synthetic procedures are shown in the Supporting Information. Complex **1** was synthesized by the reaction of platinum(II) dimer $[Pt(tfmpy)(Cl)]_2$ with an excess of *n*-$Bu_4N^+CN^-$ in CH_2Cl_2 at 50 °C for 5 h. The complex obtained was characterized by ^1H and ^{13}C NMR spectroscopy, MALDI-TOF mass spectrometry and X-ray crystal structure analysis. Single crystals of **1** were obtained by slow diffusion of ethyl ether to its dichloromethane solution (Figure S2, CCDC 1839766). As confirmed by X-ray crystallography, the Bu_4N^+ cations are squeezed between adjacent $[Pt(tfmpy)(CN)_2]^-$ anions, forming alternating layers of two oppositely charged ions. Figure 1b shows that the adjacent Pt complexes are separated from each other by more than 10 Å. Therefore, Pt···Pt and π-π stacking interactions are absent because of the spatial isolation of **1**.

2.2. Photoluminescence Properties

The PL properties of **1** were investigated first. As illustrated in **Figure 2**, **1** exhibited a sharp structured emission band at 479–547 nm in the solid state with a high quantum efficiency of 65.7%. The observed strong green emission can be attributed to the isolated monomer because the crystal structure of **1** shows that Pt···Pt and π-π stacking interactions are absent as a

consequence of the crystal packing caused by the bulky *n*-Bu_4N^+ cations (Figure 1b). In sharp contrast, it displays very weak PL intensity in a dilute CH_2Cl_2 solution (20 μM), corresponding to the quantum efficiency lower than 0.1%. However, increasing the volume fraction of a poor hexane solvent in the CH_2Cl_2-hexane mixed solution, the bright green light is constantly intensified, clearly demonstrating the aggregation induced phosphorescence emission (AIPE) effect of **1**. This AIPE phenomenon can be explained by an energy stabilization of quenching the d-d* states in solution due to molecular distortions and bond-length changes.[7a]

2.3. Spontaneous Self-Assembly

The self-assembling properties of **1** in CH_3CN solution were then studied. Scanning electron microscopy (SEM) and transmission electron microscopy (TEM) images in **Figures 3**a and S3 showed that the nanorods (aggregate state **A**) were formed by slow evaporation of CH_3CN solution of **1** ($c = 1 \times 10^{-4}$ M). These nanorods have been measured with the width of about 300 nm and length of about tens of micrometer. In addition, such rod-like nanostructures were characterized by an intense green PL emission, which is the same as that of the monomeric molecule of **1**. The identity of the energy and profile of the PL spectra for **1** and **A** reveals that no Pt···Pt interactions are present (Figure S5).

2.4. Electric Field Induced Assembly

It has been demonstrated that when neighbouring monomeric platinum(II) complexes interact with each other by Pt···Pt metallophilic interactions, the emission bands will exhibit significant bathochromic shifts. Thus, to realize the distinctly different morphologies and optical properties for **1**, shortening the distance between metal center of adjacent molecules is crucial. It would be an effective way to achieve this purpose by varying the spatial position of the ionic complex and the counterion *via* an electric field. Electrophoretic deposition (EPD) technique was used to guide the self-assembly of **1** on electrode surface in this study. EPD is a fast and convenient method that involves the movement of ionic molecules under an

appropriate external electric field.[9] Here, two aluminum foil wrapped Pt electrodes were immersed in a CH_3CN solution of **1** (1×10^{-4} M). From **Figure 6**a, we can see that the CH_3CN solution of **1** is almost non-emissive under 365 nm irradiation. Upon applying a voltage of 3 V for 60 seconds, a bright orange emission can be discerned on the anode under the UV light at 365 nm. From the mass spectral data of **1** on the anode, we can see that the structure of **1** remains intact under our experimental conditions (Figures S6). It clearly demonstrated that such an emission is originated from the triplet metal-metal-to-ligand charge transfer (^{3}MMLCT) states, which is associated with the Pt···Pt metallophilic interactions. Moreover, the appearance of MMLCT absorption band at 451 nm further reveals the Pt···Pt interactions between adjacent monomers of **1** (Figure S7). This interesting electric field induced changes in morphology and luminescence should be promising in realizing information recording and data security protection systems.[10]

In addition to distinct luminescence changes of **1** after applying an external electric field, the supramolecular structure of **1** has been noticeably altered as well. A flower-like assembly (aggregate state **B**) with a mean diameter of 5 μm was observed in the SEM image as shown in Figures 3b and S8. It suggests that these flower-like assemblies are three-dimensional hierarchically assembled supramolecular architectures, which were constructed by a large number of ultrathin nanoribbons. To gain a further insight into the aggregate state **B**, a grid net was used to replace the Pt electrode as the anode to facilitate TEM investigation. After applying a voltage of 3 V for 60 seconds, a bright orange luminescence was observed on the grid net as expected. TEM images in Figures 3d, S4 and S9 confirmed that the flower-like structures consist of numerous ultrathin nanoribbons. The thickness of nanoribbon was measured by atomic force microscopy (AFM). From its cross-sectional analysis, it was found that the thickness is approximately 6 nm as shown in Figure 3f. Furthermore, the presence and uniform distribution of carbon, nitrogen, fluorine, and platinum in the flower-like

supramolecular nanostructures were confirmed by the corresponding elemental mapping (**Figure 4**).

2.5. Effect of Electric Field and Electrodes

The investigations of the effect of the electric field on the molecular assembly have been carried out. Firstly, the supramolecular structures of **1** under different voltages have been studied. In Figure S10, SEM images of aggregate state **B**, which was formed by applying different voltages of 3, 5, 7, and 9 V, showed similar supramolecular structures, indicative of the fact that the influence of voltage on the morphology of **1** can be ignored. Besides, the structural evolution with variation of the voltage application time (15 s, 30 s, 45 s and 60 s) was observed for the samples in SEM images, which clearly showed the stepwise growth mechanism of aggregate state **B** of **1** (**Figure 5**). The influence of different electrodes on the formation of nanostructures has also been studied. Figure S11 shows that different electrodes have notable effects on the self-assembled structures. Thick nanosheets were observed by using copper as the electrode at a certain voltage. When indium tin oxide (ITO) was used as the electrode, irregular nanoparticles were formed by applying a voltage.

2.6. Molecular Packing

It is believed that the spatial location of bulky cations of Bu_4N^+ is critical for growing the different nanostructures of **1**. For aggregate state **A**, selected area electron diffraction (SAED) and powder X-ray diffraction (PXRD) analysis suggest that these nanorods have high crystallinity. In Figure 3e, the diffraction peaks of nanorods well matched with the calculated data by Mercury from the single-crystal data of **1**. It is strongly suggested that the molecular packing of nanorod is similar to that of the single crystal of **1**, and the Bu_4N^+ cations are squeezed between adjacent platinum(II) complex anions, forming alternating layers of two ions (Figure 6b). For aggregate state **B**, SAED analysis of multiple stacked region of aggregate state **B** exhibited obvious diffraction rings, which confirms its crystalline nature (Figure 3c). It is worth noting that one *d* spacing is about 0.36 nm (Figure S12), which is

indicative of the presence of periodic Pt···Pt and π-π stacking interactions in the self-assembled materials. In addition, the change in emission lifetimes between aggregate state **A** and **B** can also confirm the formation of intermolecular Pt···Pt and π-π stacking interactions in the flower-like nanostructure (Figure S13). Therefore, it is believed that the ultrathin nanoribbon is constructed by a layer-by-layer packing through the formation of Pt···Pt and π-π stacking interactions, which is schematically depicted in Figure 6b.

SAED analysis and emission lifetime measurement of the assembled structures on different electrodes have been performed. In Figure S14, we can see that SAED analysis of the thick nanosheets obtained on the copper electrode showed obvious diffraction rings, which confirms its crystalline nature. In these assemblies, one *d* spacing was calculated as 0.36 nm, indicating the presence of periodic Pt···Pt and π–π stacking interactions. Besides, the emission lifetime of these thick nanosheets is similar to that of aggregate state **B** (Figure S13), which confirms that the molecular packing of the two nanostructures is the same. However, as shown in Figure S14, SAED analysis revealed the amorphous nature of the irregular nanoparticles obtained on the ITO electrode. Emission decay time of these irregular nanoparticles is different from that of the aggregate state **B** (Figure S13). These results indicate the different molecular packing of irregular nanoparticles from aggregate state **B**. The differences in surface roughness of various electrodes may be responsible for the different supramolecular structures. Nucleation and oriented growth of molecules on the ITO electrode is difficult because of its very smooth surface and low surface energy. As a result, amorphous irregular nanoparticles are likely to grow on the ITO electrode. Based on these results, we can conclude that electric filed is indeed a decisive factor in forming different nanostructures.

2.7. Confocal Fluorescence Imaging

Confocal fluorescence microscopy (CFM) was utilized to study the changes of morphologies and emission colors of assemblies. As shown in **Figure 7**a, the sample prepared by evaporation of a CH_3CN solution of **1** exhibited a rod-like supramolecular nanostructure with

a strong green emission at an excitation wavelength of 405 nm that corresponds to assembly **A**. In contrast, flower-shaped assembly **B** shows an intense orange emission maximum at 587 nm (Figure 7b). Also, photoluminescence lifetime imaging microscopy (PLIM) was utilized to examine the emission decay time change. The lifetime imaging clearly illustrates that the emission lifetime significantly decreased from 900 ns to 280 ns after formation of intermolecular Pt···Pt and π-π stacking interactions of **1** (Figures 7c and 7d). This change is in accordance with the previous report.[11] Therefore, we are able to distinguish the difference in supramolecular structures of **1** according to their optical variations.

3. Conclusion

To conclude, we have demonstrated that the utilization of external electric field could be an effective way to create supramolecular architectures. For **1**, electric field markedly helped it to overcome the steric hindrance of bulky counterion to assemble into flower-shaped nanostructures. SEM and TEM images reveal that the flower-like superstructures are composed of numerous ultrathin nanoribbons. Moreover, it was found that these two stable morphologies possess distinct luminescence properties. Our results suggest that it could be a reliable method in charged self-assembling systems by the introduction of electric field to help construct nanostructures. It may be promising in various optoelectronic applications, such as data recording, anti-counterfeiting, smart windows, and so on.

4. Experimental Section

Materials: Unless otherwise stated, all starting materials and reagents were purchased from commercial suppliers and used without further purification. All solvents were purified before use. The solvents were carefully dried and distilled from appropriate drying agents prior to use.

Measurements: NMR (^{1}H: 400 MHz, ^{13}C: 100 MHz) spectra were recorded on a Bruker ACF400 spectrometer at 298 K using deuterated solvents. Mass spectra were obtained on a Bruker autoflex matrix-assisted laser desorption ionization time-of-flight (MALDI-TOF/TOF)

mass spectrometer. UV-visible absorption spectra were recorded with a Shimadzu UV-2600 spectrophotometer. Photoluminescent spectra were measured with an Edinburgh Instrument FLS920. The fluorescence quantum efficiency of the solid state was measured on a FLS920 steady state and calibrated integrating sphere systems from an Edinburgh Instrument. X-Ray diffraction data were collected at 293 K using graphite-monochromated Mo−Kα radiation (λ = 0.71073 Å) on a Bruker APEX DUO diffractometer. The collected frames were processed with the software SAINT and an absorption correction (SADABS) was applied to the collected reflections. The structure was solved by the Direct methods (SHELXTL) in conjunction with standard difference Fourier techniques and subsequently refined by full-matrix least-squares analyses on F_2.

Photoluminescence lifetime imaging: The obtained nanostructures were placed on the PLIM setup, which is integrated with Olympus IX81 laser scanning confocal microscope. The photoluminescence signal was detected by the system of the confocal microscope and correlative calculation of the data was carried out by professional software which was provided by Pico Quant Company. The light from the pulse diode laser head (Pico Quant, PDL 800-D) with excitation wavelength of 405 nm and frequency of 0.5 MHz was focused onto the sample with a 40x/NA 0.95 objective lens for single-photon excitation.

Synthesis of 1: A mixture of platinum(II) bis(2-(4-(trifluoromethyl)phenyl)pyridine) dichloro-bridged dimer (0.1 mmol) and an excess of tetrabutylammonium cyanide (0.5 mmol) was dissolved in dichloromethane at 50 °C for 3 h. The solvent was removed and the residue was washed with water and extracted with dichloromethane. Then, the product was recrystallized by vapor diffusion of diethyl ether into dichloromethane. Yield 71%. ^{1}H NMR (400 MHz, $CDCl_3$): (ppm) 9.51 (d, J = 4 Hz, 1H), 8.45 (s, 4H), 7.92 (t, J = 8 Hz, 1H), 7.78 (d, J = 8 Hz, 1H), 7.60 (d, J = 8 Hz, 1H), 7.34 (d, J = 8 Hz, 1H), 7.22 (t, J = 8 Hz, 1H). 3.37–3.33 (m, 8H), 1.74–1.66 (m, 8H), 1.52–1.43 (m, 8H), 1.01 (t, J = 8 Hz, 12H). ^{13}C NMR (100 MHz, $CDCl_3$), (ppm): 166.49, 158.03, 153.33, 150.14, 139.14, 134.87, 131.23, 130.39, 125.97, 123.89,

123.26, 122.94, 120.68, 119.45, 58.80, 24.01, 19.62, 13.62. MS (MALDI-TOF) [m/z]: 468.6 $[M-Bu_4N]^-$.

Supporting Information

Supporting Information is available from the Wiley Online Library or from the author.

Acknowledgements

We are grateful to the financial support from the Hong Kong Research Grants Council (PolyU 153062/18P), the Hong Kong Polytechnic University (1-ZE1C), Ms Clarea Au for the Endowed Professorship (847S), Natural Science Foundation of Jiangsu Province of China (BK20160885), the National Program for Support of Top-Notch Young Professionals, the National Natural Science Foundation of China (21701087, 21671061 and 61804082), and the China Postdoctoral Science Foundation funded project (2018M642286).

Received: ((will be filled in by the editorial staff))
Revised: ((will be filled in by the editorial staff))
Published online: ((will be filled in by the editorial staff))

References

[1] a) J. M. Lehn, *Science* **2002**, *295*, 2400–2403. b) T. Aida, E. W. Meijer, S. I. Stupp, *Science* **2012**, *335*, 813–817. c) A. Aliprandi, M. Mauro., L. D. Cola, *Nat. Chem*. **2016**, *8*, 10–15.

[2] a) P. K. Kundu, D. Samanta, R. Leizrowice, B. Margulis, H. Zhao, M. Börner, T. Udayabhaskararao, D. Manna, R. Klajn, *Nat. Chem*. **2015**, *7*, 646–652. b) Y. S. Cai, Z. Q. Guo, J. M. Chen, W. L. Li, L. B. Zhong, Y. Gao, L. Jiang, L. F. Chi, H. Tian, W. H. Zhu, *J. Am. Chem. Soc*. **2016**, *138*, 2219–2224. c) X. Li, J. Fei, Y. Xu, D. Li, T Yuan *Angew. Chem. Int. Ed.* **2018**, *57*, 1903–1907.

[3] a) R. Klajn, P. J. Wesson, K. J. M. Bishop, B. A. Grzybowski, *Angew. Chem. Int. Ed.* **2009**, *48*, 7035–7039. b) G. Singh, H. Chan, A. Baskin, E. Gelman, N. Repnin, P. Král, R. Klajn. *Science* **2014**, *345*, 1149–1153. c) M. Vilfan, A. Potocnik, B. Kavcic, N. Osterman, I. Poberaj, A. Vilfan, D. Babic, *Proc. Natl. Acad. Sci. USA* **2010**, *107*, 1844–1847.

[4] a) Y. Shoji, M. Yoshio, T. Yasuda, M. Funahashi, T. Kato, *J. Mater. Chem.* **2010**, *20*, 173–179. b) Y. S. Velichko, J. R. Mantei, R. Bitton, D. Carvajal, K. R. Shull, S. I. Stupp, *Adv. Funct. Mater.* **2012**, *22*, 369–377. c) Q. B. Zhang, K. B. Yin, H. Dong, Y. L. Zhou, X. D. Tan, K. H. Yu, X. H. Hu, T. Xu, C. Zhu, W. W. Xia, F. Xu, H. M. Zheng, L. T. Sun, *Nat. Commun*. **2017**, *8*, 14889. d) F. D. Ma, S. J. Wang, D. T. Wu, N. Wu, *Proc. Natl. Acad. Sci. USA* **2015**, *112*, 6307–6312.

[5] a) C. Po, A. Y. Y. Tam, K. M. C. Wong, V. W. W. Yam, *J. Am. Chem. Soc*. **2011**, *133*, 12136–12143. b) C. Po, V. W. W. Yam, *Chem. Sci.* **2014**, *5*, 4868–4872. c) K. P. Guo, F. Zhang, S. Guo, K. Li, X. Q. Lu, J. Li, H. Wang, J. Cheng, Q. Zhao, *Chem. Commun*. **2017**, *53*, 1309–1312.

[6] a) A. Aliprandi, D. Genovese, M. Mauro, L. D. Cola, *Chem. Lett*. **2015**, *44*, 1152–1169. b) P. Chow, G. Cheng, G. S. M. Tong, W. To, W. Kwong, K. Low, C. Kwok, C. S. Ma, C.-M. Che, *Angew. Chem. Int. Ed.* **2015**, *54*, 2084–2089. c) F. Camerel, R. Ziessel, B. Donnio, C. Bourgogne, D. Guillon, M. Schmutz, C. Iacovita, J. Bucher, *Angew. Chem. Int. Ed.* **2007**, *46*, 2659–2662.

[7] a) A. F. Rausch, U. V. Monkowius, M. Zabel, H. Yersin, *Inorg. Chem.* **2010**, *49*, 7818–7825. b) J. Forniés, S. Fuertes, J. A. López, A. MartÍn, V. Sicilia, *Inorg. Chem.* **2008**, *47*, 7166–7176.

[8] a) Z. X. Xu, X. D. Zhuang, C. Q. Yang, J. Cao, Z. Q. Yao, Y. P. Tang, J. Z. Jiang, D. Q. Wu, X. L. Feng, *Adv. Mater*. **2016**, *28*, 1981–1987. b) M. Salimimarand, D. D. La, M. A. Kobaisi, S. V. Bhosale, *Sci. Rep*. **2017**, *7*, 42898.

[9] a) R. A. Masitas, S. L. Allen, F. P. Zamborini, *J. Am. Chem. Soc.* **2016**, *138*, 15295–15298. b) Q. Chen, R. P. Garcia, J. Munoz, L. U. Pérez, N. Garmendia, Q. Yao, A. R. Boccaccini, *ACS Appl. Mater. Interfaces* **2015**, *7*, 24715–24725

[10] a) K. Y. Zhang, X. J. Chen, G. L. Sun, T. W. Zhang, S. J. Liu, Q. Zhao, W. Huang, *Adv. Mater*. **2016**, *28*, 7137–7142. b) H. B. Sun, S. J. Liu, W. P. Lin, K. Y. Zhang, W. Lv, X.

Huang, F. W. Huo, H. R. Yang, G. Jenkins, Q. Zhao and W. Huang, *Nat. Commun.* **2014**, *5*, 3601. c) Y. Ma, S. Liu, H. Yang, Z. Yi, P. She, N. Zhu, C. L. Ho, Z. Qiang, H. Wei and W. Y. Wong, *Inorg. Chem.* **2017**, *56*, 2409–2416.

[11] a) W. Lu, Y. Chen, V. A. L. Roy, S. S. Y. Chui, C. M. Che, *Angew. Chem. Int. Ed.* **2009**, *48*, 7621-7625. b) K. M. C. Wong, V. W. W. Yam, *Acc. Chem. Res.* **2011**, *44*, 424–434.

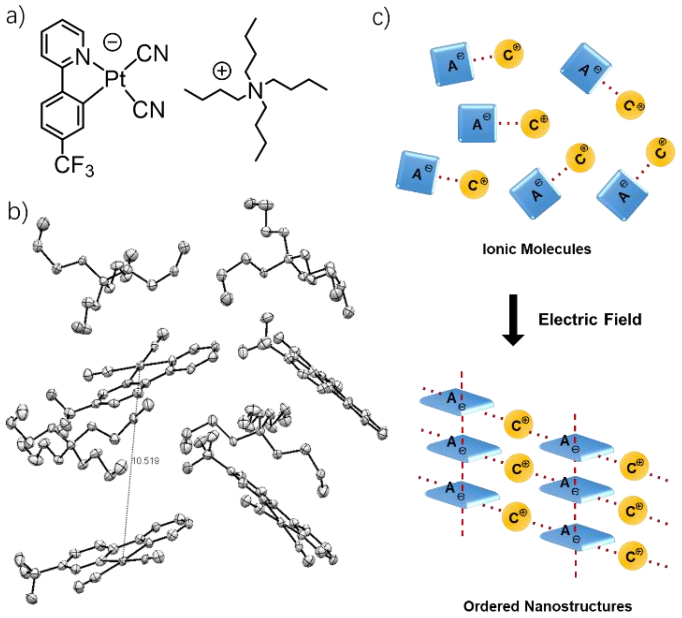

Figure 1. a) Chemical structure of complex **1**. b) A perpendicular view illustrating the alternation of *n*-Bu_4N^+ cations and Pt complex anions within the crystal of **1**. The Pt···Pt separation amounts to 10.519 Å. c) Schematic diagram showing the utilization of electric field to control the self-assembly of ionic molecules to form ordered nanostructures.

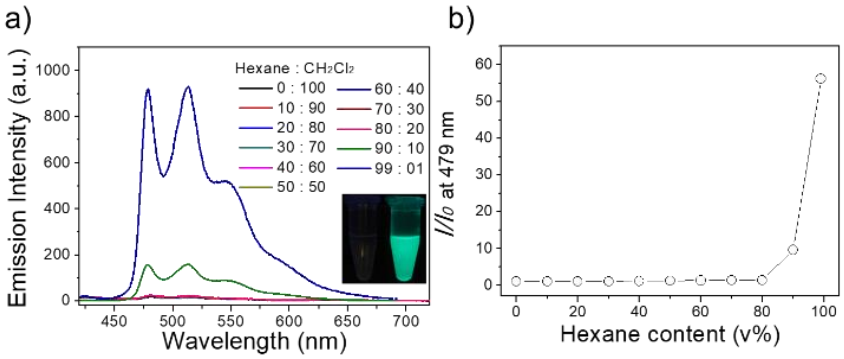

Figure 2. a) PL spectra of **1** in hexane–CH_2Cl_2 mixtures (20 μM) with different hexane fractions. Inset: photographs of **1** in CH_2Cl_2 (left) and hexane–CH_2Cl_2 mixture (*v* : *v*, 99 : 1) (right) under 365 nm irradiation. b) A plot of the relative PL intensity (I/I_0) of **1** at 479 nm versus the composition of the hexane–CH_2Cl_2 mixture of **1** (I_0 is the PL intensity in pure CH_2Cl_2 solution).

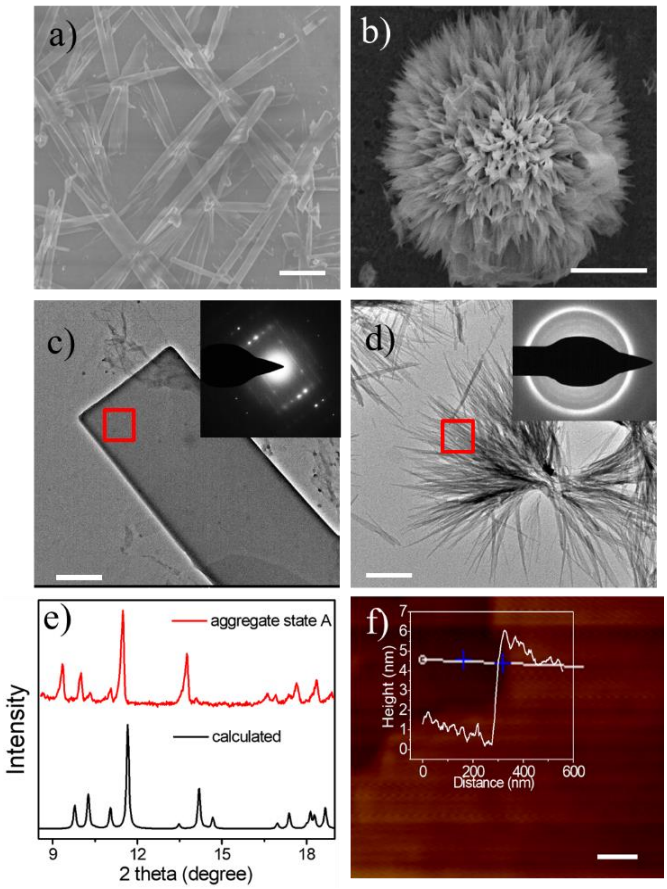

Figure 3. a) SEM image prepared by slow evaporation of a CH_3CN solution of **1** (1×10^{-4} M). Scale bar = 10 μm. b) SEM images prepared by applying a voltage of 3 V for 60 seconds in a CH_3CN solution of **1** (1×10^{-4} M). Scale bar = 3 μm. c) TEM image and the corresponding SAED patterns (inset) of the aggregate state **A**. Scale bar = 1 μm. d) TEM image and the corresponding SAED patterns (inset) of aggregate state **B**. Scale bar = 1 μm. e) PXRD patterns of the nanorods (red line) and the calculated data by Mercury from the single-crystal data of complex **1** (black line). f) AFM image and its cross-section analysis of nanoribbon structure. Scale bar = 100 nm

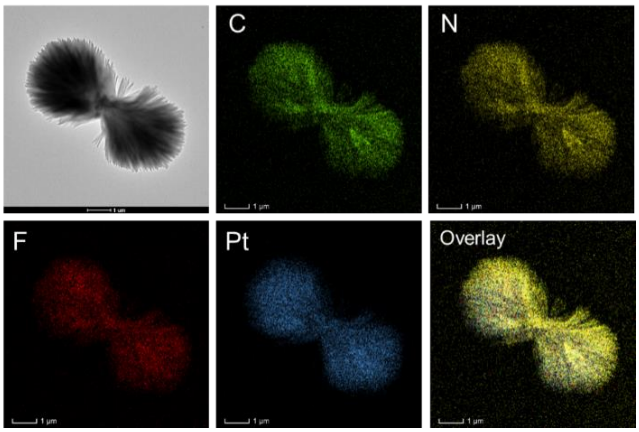

Figure 4. Energy-dispersive X-ray spectroscopy analysis of typical flower-like nanostructure and the corresponding elemental mapping.

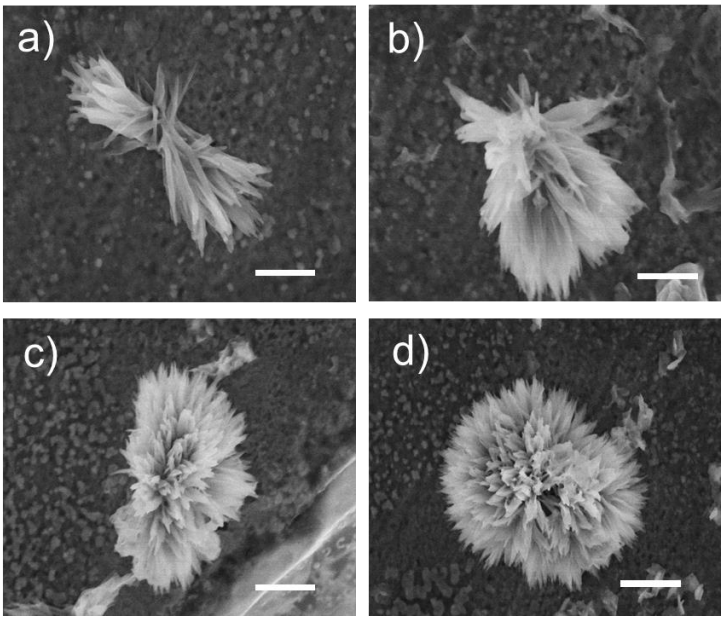

Figure 5. SEM images of the flower-like nanoaggregate at various stages of growth. a) 15 s, b) 30 s, c) 45 s, and d) 60 s. Scale bar = 2 μm.

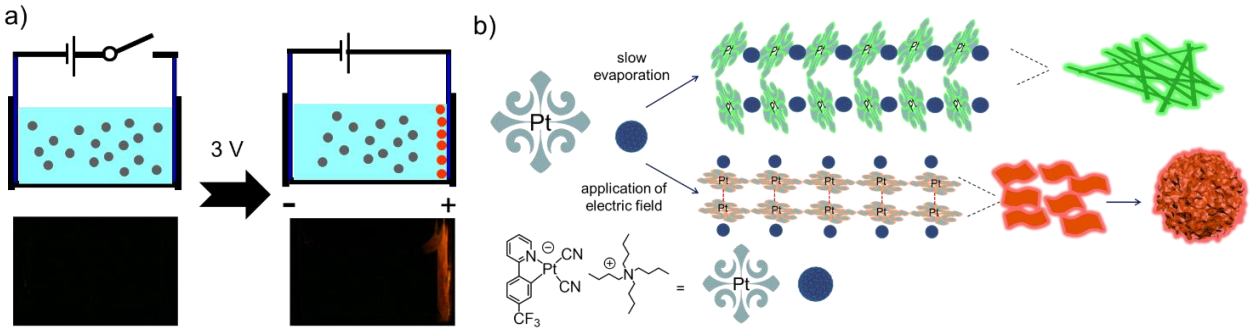

Figure 6. a) Diagram illustrating the setup for the investigation of the luminescence change of **1** under electric field and photographs of **1** (10×10^{-4} M) in acetonitrile before and after applying a voltage of 3 V under photoexcitation at 365 nm. b) Schematic diagram showing the formation of the rod-like and flower-like nanostructure of **1**

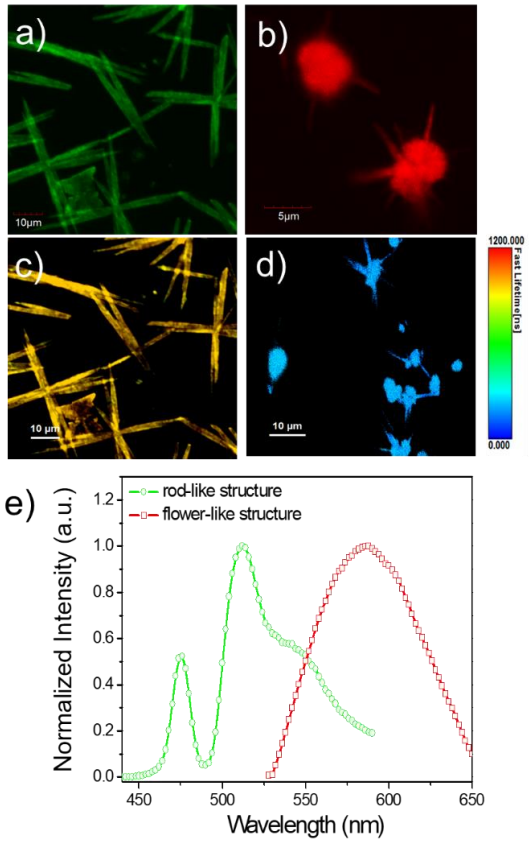

Figure 7. CFM images of a) rod-like and b) flower-shaped nanostructures. PLIM images of c) rod-like and d) flower-shaped supramolecular structures. e) PL spectra obtained by CFM.

The table of contents

The self-assembly of an anionic platinum complex ([Pt(tfmpy)(CN)$_2$]$^-$Bu$_4$N$^+$) in the absence or presence of an electric field has been studied in this work. SEM and TEM images demonstrated an interesting morphological transformation from rod-like to flower-shaped nanoaggregate structure. Importantly, it is found that these two different stable assemblies possess distinct emission colors.

Keyword: supramolecular chemistry, molecular assembly, metal-metal interactions, electric field, photoluminescence

Yun Ma, Weiwei Zhao, Pengfei She, Suyi Liu, Liang Shen, Xiangling Li, Shujuan Liu, Qiang Zhao*, Wei Huang, and Wai-Yeung Wong*

Electric Field Induced Molecular Assemblies Showing Different Nanostructures and Distinct Emission Colors